Biological Cybernetics (2018) 112:165–179
https://doi.org/10.1007/s00422-017-0742-x

Biological Cybernetics

ORIGINAL ARTICLE

Identification of optimal feedback control rules from micro-quadrotor and insect flight trajectories

Imraan A. Faruque[1] · Florian T. Muijres[3] · Kenneth M. Macfarlane[2] · Andrew Kehlenbeck[2] · J. Sean Humbert[4]

Received: 24 August 2016 / Accepted: 8 December 2017 / Published online: 3 January 2018

Abstract
This paper presents "optimal identification," a framework for using experimental data to identify the optimality conditions associated with the feedback control law implemented in the measurements. The technique compares closed loop trajectory measurements against a reduced order model of the open loop dynamics, and uses linear matrix inequalities to solve an inverse optimal control problem as a convex optimization that estimates the controller optimality conditions. In this study, the optimal identification technique is applied to two examples, that of a millimeter-scale micro-quadrotor with an engineered controller on board, and the example of a population of freely flying *Drosophila hydei* maneuvering about forward flight. The micro-quadrotor results show that the performance indices used to design an optimal flight control law for a micro-quadrotor may be recovered from the closed loop simulated flight trajectories, and the *Drosophila* results indicate that the combined effect of the insect longitudinal flight control sensing and feedback acts principally to regulate pitch rate.

Keywords Insect · Flight · Control · Optimal · Identification · Drosophila

1 Introduction

Many biological control structures exhibit performance and robustness properties that exceed engineered systems, and biologically-inspired studies are a potential source for new methods of controlling engineered problems. A common problem in many of these studies is testing hypotheses of how a neural structure processes information. Typically, these hypotheses are compared using statistical methods or root-mean-square comparisons of the degree to which predictive models match some other data. Control-theoretic approaches that can efficiently reduce a library of automatically-measured motions into an underlying control model are applicable to such problems.

Flying insect control is an example of natural performance, since many species of insects are capable of robustly navigating through unknown environments while using extremely constrained neural resources. A detailed model of the mechanisms by which this stabilization and control is achieved would provide a significant contribution to the understanding of insect-based flight control, and the ability to replicate this robust control of flight performance would represent a significant leap forward in the control of vehicles having strict size, weight, and power (SWaP) limitations. Biologically motivated design principles for feedback control could unlock substantial improvements in the control of engineered flight at the micro aerial vehicle (MAV) scale. In particular, a detailed understanding of the overall performance of the insect's onboard feedback controller could provide critical insight into the associated sensing requirements of an insect's feedback strategy, and eventually allow engineered controllers

This work sponsored in part by the US Air Force Office of Scientific Research (FA95501410068) and by the US Army Research Laboratory (W911NF-08-2-0004). Special thanks to Prof. Michael Dickinson's laboratory at Caltech for providing the *Drosophila* data for analysis.

✉ Imraan A. Faruque
i.faruque@okstate.edu

[1] School of Mechanical and Aerospace Engineering, Oklahoma State University, Stillwater, OK, USA

[2] Department of Aerospace Engineering, University of Maryland, College Park, MD, USA

[3] WU Animal Sciences,Wageningen UR, Wageningen, The Netherlands

[4] Department of Mechanical Engineering, University of Colorado, Boulder, CO, USA

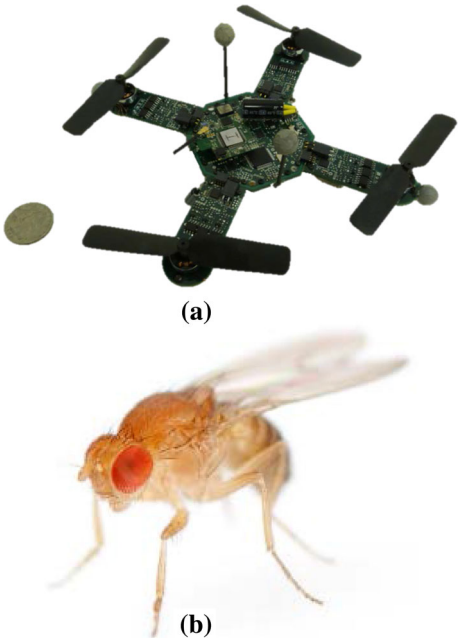

Fig. 1 An engineered and a biological flight platform were selected for feedback control optimality extraction via the optimal identification (OID) technique

that are tuned to achieve the same closed loop performance targets.

In this study, a novel control-theoretic technique called "optimal identification" (OID) is introduced and applied to a small-scale quadrotor, Fig. 1a, and to measurements of insects, Fig. 1b, in free flight, establishing a method of extracting a flight control law and biologically-relevant design principles from flight trajectory measurements. The technique combines reduced order open loop flight dynamics modeling, closed loop system identification, feedback control law extraction, and a linear matrix equality formulation of the solution to the inverse optimal control problem. The result is a set of optimality conditions that allows researchers to quantify the relative performance of the insect's control law, weighted against the control input deviations required to achieve such performance. The insect optimality conditions may be used in the goal of translating insect control laws into engineered systems through the use of existing optimal control design techniques.

This paper is structured as follows. Section 2 reviews previous work on insect based flight control. Section 3 describes the approach as a 4-part "optimal identification" method involving open loop modeling, closed loop measurement, feedback control extraction, and inverse optimal control. Section 4 describes the methods by which the trajectory data were gathered for the example platforms studied. Section 5 presents the results of each of the four OID stages, including a comparison of several individual insects' feedback control strategies.

2 Background and previous work

Insect flight control systems incorporate specialized arrays of sensing and actuation systems. The visual system, consisting of the compound eyes (Wehner 1981; Heisenberg and Wolf 2013) and the ocelli (Krapp 2009), the antennae (Schneider 1964; Sane et al. 2007), and the network of mechanosensors on the head, body and wings (Weis-Fogh 1949; Dickinson 1990) are all involved in flight control response. Dipteran insect feedback systems also incorporate halteres, a set of oscillating appendages analogous to hind wings which may operate as biological gyroscopes (Pringle 1948; Thompson et al. 2008). The strain sensors at the base of the wings of non-dipteran insects may also quantify gyroscopic forces (Thompson et al. 2008; Eberle et al. 2015). Flying insects actuate their wings through large power muscles in the thorax and small control muscles at the base of each wing. Together, these muscles allow the insect to adjust the wingbeat pattern precisely and on a stroke-to-stroke basis (Dickinson and Tu 1997), providing small, subtle changes in wingbeat pattern that alter the aerodynamic forces and moments on each wing and modulate the wingbeat-average forces and torques about the center of mass of the insect (Muijres et al. 2014). In addition, many larger flying insects actuate their hind legs or abdomen (Camhi 1970), which may produce control torques.

Flight control systems are often modeled as a high speed inner loop involved in stabilization and an outer loop control system involved in navigation or behavioral responses (Dickinson and Muijres 2016). The outer loop system is used to perform behavioral flight responses such as search maneuvers during plume tracking (Breugel and Dickinson 2014; Kennedy 1983), evasive maneuvers (Muijres et al. 2014), and landing responses (Breugel and Dickinson 2012). The inner loop system works to negate external or internal perturbations during flight, and is therefore used to regulate an insect to a trajectory or flight condition. For example, the inner loop allows insects to regulate their flight velocity (David 1978) and heading (Götz 1968), to maintain a stable body posture (Sherman and Dickinson 2003), and to remain at a desired height (Straw et al. 2010). In this study we will focus on the dynamics and design of this inner loop system, particularly the sub-systems that allow insects to stabilize flight and regulate heading.

Control of yaw axis rotations has received the most extensive study. Early research into yaw dynamics of flying insects focused on open loop flight responses where tethered fruit flies were presented with various visual inputs and compensatory wing motions were measured (Götz 1968). These experiments were followed by tethered closed loop experiments whereby maneuver responses of tethered fruit flies were fed back to the presented visual patterns, by allowing the fly to freely rotate about its yaw axis, or by measuring either yaw torques (Dickinson and Lighton 1995) or changes

in wingbeat pattern (Götz 1987) to quantify changes in maneuvers. The flight responses in tethered animals may be different from those of freely flying insects, and more recent experimental work has focused on free flight control dynamics, both experimentally and via modelling (Ristroph et al. 2010). The combined experimental and modeling work on yaw control has indicated that dipteran flapping wing insect flight involves a passive aerodynamic mechanism (Faruque and Humbert 2010a; Hedrick and Robinson 2010) that stabilizes yaw movement dynamics. As a result, yaw movements in flying insects are highly damped, which might simplify yaw control. For example, flying fruit flies require only a simple proportional-derivative controller for yaw stabilization, in which the fly feeds back deviations in sideslip angle and yaw rate to subtle changes in wingbeat average angle-of-attack (Ristroph et al. 2010).

In contrast with the highly damped yaw dynamics, pitch and roll dynamics in many flying insects are underdamped and inherently unstable. Open loop models of flying locusts (Taylor and Thomas 2003) indicated that longitudinal flight control requires more sophisticated feedback. Ristroph et al. (2013) predicts that the requirement for more involved control structures persists for a range of other flying insects, hummingbirds, and even flapping micro air vehicles. Roll dynamics can be the least damped and thus most unstable flight mode, as indicated by experimental perturbations of freely flying flies along the roll axis (Beatus et al. 2015). Analysis of the response dynamics showed agreement with proportional-integral controllers. Halteres are involved in measurement of roll rates, but their low sensitivity to small roll velocities results in a poor signal to noise ratio, and integration of this noise may be problematic. Therefore, additional sensory inputs, such as those from the visual system, are required. The changes in wingbeat pattern responsible for producing compensatory roll torques are strikingly small and similar to the kinematics changes found for flies that perform roll maneuvers during banked turns (Muijres et al. 2015), highlighting the precision with which flying insects need to adjust the wingbeat pattern for active flight control. While previous studies have focused on the individual sub-systems of the insect flight control system, in natural conditions these sub-systems are often strongly coupled and the composite function and performance of the flight control system may not be a natural extension of each individual block. Therefore, a number of studies have begun to address the free flight dynamics of flying insects, whereby open loop flight dynamics about all six degrees-of-freedom (DoF) were modeled. For these studies, the aerodynamic forces on the animal need to be modeled, as these forces are largely responsible for the open loop flight dynamics. Faruque and Humbert (2010a, b) and Cheng et al. (2010) used curve-fitted quasi-steady aerodynamics models Sane (2003); Fry et al. (2003), while Liu and colleagues (Gao et al. 2011) used computational fluid dynamics (CFD) to extract numerical models. These studies provide useful insight into the stability of different eigenmodes of body movements as well as the degree of coupling of various body rotations, but the results describe only the open-loop, or uncontrolled dynamics of the system. Since biological examples of insect flight control invariably incorporate closed loop feedback control, a generalized framework for studying the combined flight control responses would facilitate a much more representative study of natural flight.

While the sensing aspect of insect flight control has been studied both experimentally and via analytic and computational modeling, the exact form of feedback used to fuse each sensor output into a unified controller remains unknown. Sherman and Dickinson (2004, 2003) hypothesized that linear summation of visual and mechanosensory feedback was used to fuse experimental measurements taken on the respective responses for single axes, and engineering synthesis of controllers that make use of bio-inspired sensors has been demonstrated (Conroy et al. 2009). The method by which insects fuse their individual responses to combined state perturbations are not known, nor are the relative gain structures of the control strategies.

A method for deriving experimental data-driven models of the flight controller, such as controller form, cross couplings, and relative gains, could provide an understanding of how the insect's flight controller responds to composite perturbations in multiple states. Such data-based controller models could be used to quantitatively estimate the sensor performance requirements (e.g., bandwidth, noise level) needed to robustly implement an insect control strategy. Inverse optimal control approaches, first proposed for single input systems in Kalman (1964), provide a possible mechanism to interpret the combined effect of a sensing and feedback control strategy on the open loop flight dynamics. In this work, we introduce optimal identification, a method of estimating the onboard flight controller and interpreting the flight controller's effects on, or optimality with respect to, the open loop plant dynamics.

3 Approach, derivation, and modeling

This section describes the optimal identification approach generally, and then derives and describes its four components in sequence. In this work, we address systems with the general plant and controller interconnection structure shown in Fig. 2a. In these systems, we have a model $\hat{P}$ of the open loop plant dynamics P, while we assume the sensing and feedback system K is unknown.

We seek to use our open loop model $\hat{P}$, combined with measurements of the state perturbations $\mathbf{x}(t)$ and control perturbations $\mathbf{u}(t)$, to reverse engineer the flight controller $\hat{K}$

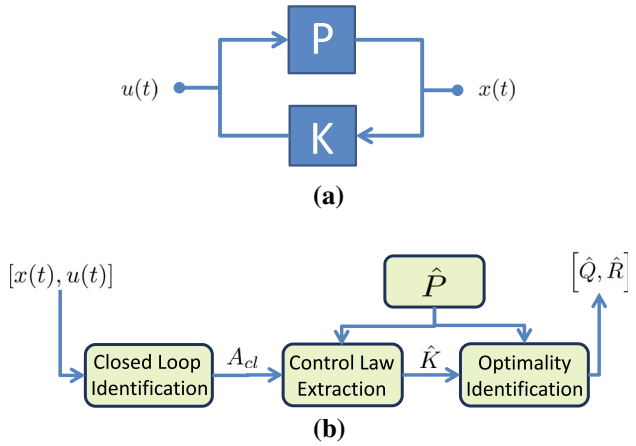

Fig. 2 Block diagram of the general optimal identification approach, showing closed loop time-histories of state $\mathbf{x}(t)$ and $\mathbf{u}(t)$, which may be used to identify a control law $\hat{K}$ and the optimal control design matrices $(\hat{Q}, \hat{R})$

for both an engineered (microquadrotor) and natural (insect) system. We first break the process of estimating and interpreting the controller $\hat{K}$ into four components as shown in Fig 2b: open loop flight dynamics modeling, closed loop flight dynamics system identification, feedback control law extraction, and optimal control inversion.

Figure 3 applies the general form shown in Fig. 2b to insect flight control study. Optimal identification is useful to determine the combined effect of the sensing and control block, i.e., the combined sensing and control relationship between **x** and **u**, shown as a dashed box in Fig. 3.

3.1 Open loop dynamics modeling

The open loop dynamics model $\hat{P}$ forms a reference by which one can estimate the effects of closed loop control. Recent reduced order models of flight dynamics based on quasi-steady aerodynamics, wingstroke averaging, and linearization have shown promise at describing the uncontrolled insect flight system (Hedrick et al. 2009; Faruque and Humbert 2010b). The model applied in this study utilizes experimentally-derived aerodynamic coefficients for a *Drosophila* wing and a quasi-steady assumption to estimate aerodynamic loading with varying wing kinematics (Dickinson et al. 1954). Changes in stroke averaged loads during perturbations from a reference flight condition are used to construct a linear dynamical model according to small perturbation analysis, an approach that has been shown to extract open loop dynamics similar to those produced by computationally expensive CFD techniques (Sun et al. 2007; Gao et al. 2011; MacFarlane et al. 2011). Similarly, control input perturbations may be used to quantify the aerodynamic effects of control inputs to create an input to output flight dynamics model.

Free-flying *Drosophila* insect trajectories were collected using an automated high speed camera setup and image tracking software (Muijres et al. 2014). Translational speeds (u, v, w), angular rates (p, q, r), aerodynamic forces (X, Y, Z) and torques (L, M, N) were defined relative to the stability axes $\mathcal{S} = \{\hat{s}_x, \hat{s}_y, \hat{s}_z\}$ as shown in Fig. 4. Trajectory analysis was limited to sequences involving straight and level forward flight, featuring small body pitch angle θ excursions, small accelerations, and low climb or descent speed.

A prerequisite for any linear dynamical model is the choice of kinematic reference condition. For this study, the reference condition for linear dynamical modeling was taken to be the ensemble average of all recorded wing kinematics, which were assumed to be harmonic motions. For example, left and right wing stroke angles were described by

$$\phi_R(t) = \Phi_R \cos(2\pi f t) + \phi_{off,R}, \quad (1)$$

$$\phi_L(t) = \Phi_L \cos(2\pi f t) + \phi_{off,L}. \quad (2)$$

Perturbations to the collective stroke amplitude $\Phi = \frac{1}{2}(\Phi_R + \Phi_L)$, stroke bias $\phi_{off} = \frac{1}{2}(\phi_{off,R} + \phi_{off,L})$, and stroke plane angle $\beta_c = \frac{1}{2}(\beta_R + \beta_L)$ terms in Fig. 5 were used as control

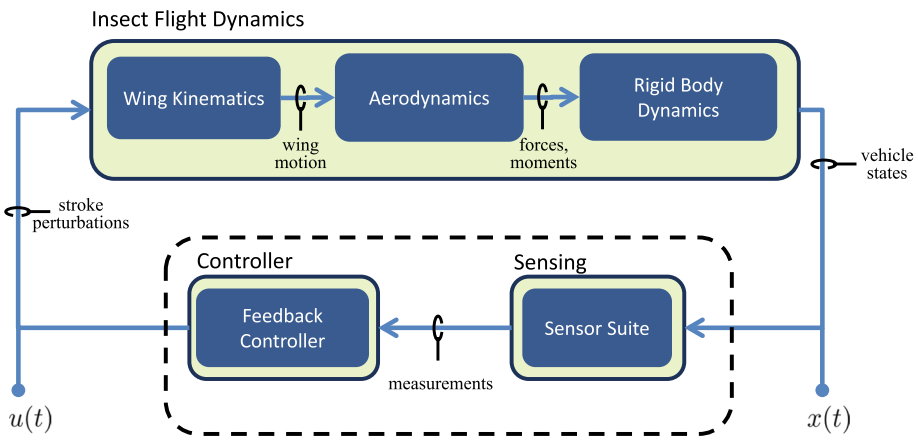

Fig. 3 Optimal identification works to extract design rules for feedback controllers from closed loop experimental data by finding a design structure for the combined control/sensing block (dashed) in the insect flight control task from state $\mathbf{x}(t)$ and input $\mathbf{u}(t)$ recordings

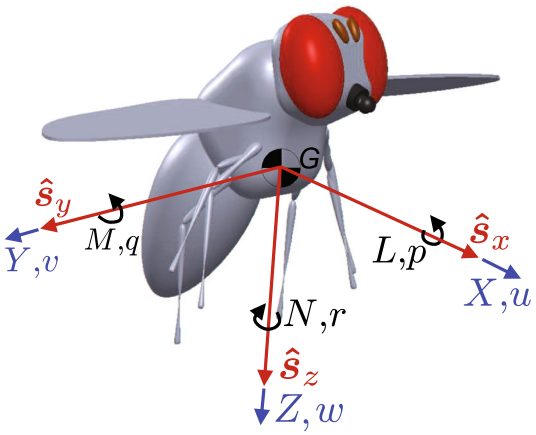

Fig. 4 Forces, torques, and translational and angular rates were defined relative to stability axes $\mathcal{S}$ passing through the center of mass G

inputs. Lateral-directional deviations such as $\beta_d = \frac{1}{2}(\beta_R - \beta_L)$ were digitized, but their effects were outside the scope of this longitudinal study.

3.2 Closed loop trajectory measurement

Some mechanism for capturing closed loop trajectories is needed as input data. Optimal identification is applicable to trajectories generated by both simulated dynamics and by experimental measurement. Section 4 presents a detailed description of the microquadrotor simulation and the hardware, methods, and experimental design used in the measurement of freely flying *Drosophila*.

3.3 Closed loop flight dynamics system identification

After trajectories from the micro-quadrotor simulation and free flight insects were collected, system identification was used to identify the closed loop dynamics. For the quadrotor, the control inputs were considered longitudinal perturbations to the rotor speeds $\mathbf{u} = (\delta_{\text{lon}}) \in [-1, 1]$, linearly related to pitch and roll rates. For the insect case, composite wingstroke parameters $\mathbf{u} = [\Phi, \beta_c, \phi_{\text{off}}]^{\text{T}}$ were used as inputs . Example

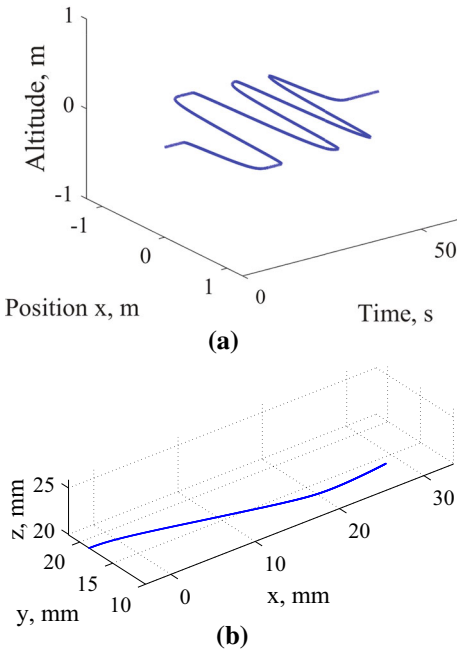

Fig. 6 Example flight trajectories used for feedback control law identification

flights used in time domain system identification for both of the platforms are shown in Fig. 6, showing longitudinal quadrotor flight and an insect in forward flight making right and left turns.

The free parameters in the longitudinal microquadrotor flight dynamics identification were (X_u, X_q, Z_u, M_{x_i}, M_x, M_u, M_q, and M_θ. The parameters in the longitudinal insect flight dynamics model were (X_u, Z_u, Z_w, M_u, M_w, M_q, X_Φ, $X_{\phi_{\text{off}}}$, M_β, Z_Φ, $Z_{\phi_{\text{off}}}$, M_Φ, $M_{\phi\text{off}}$), arranged as follows:

$$A = \begin{bmatrix} X_u & 0 & 0 & -g \\ Z_u & Z_w & 0 & 0 \\ M_u & M_w & M_q & 0 \\ 0 & 0 & 1 & 0 \end{bmatrix}, \; B = \begin{bmatrix} 0 & X_\Phi & X_{\phi_{\text{off}}} \\ 0 & Z_\Phi & Z_{\phi_{\text{off}}} \\ M_\beta & 0 & M_{\phi_{\text{off}}} \\ 0 & 0 & 0 \end{bmatrix}. \tag{3}$$

A summary of the state $\mathbf{x}$ and input $\mathbf{u}$ vectors used in this paper is included in Table 1.

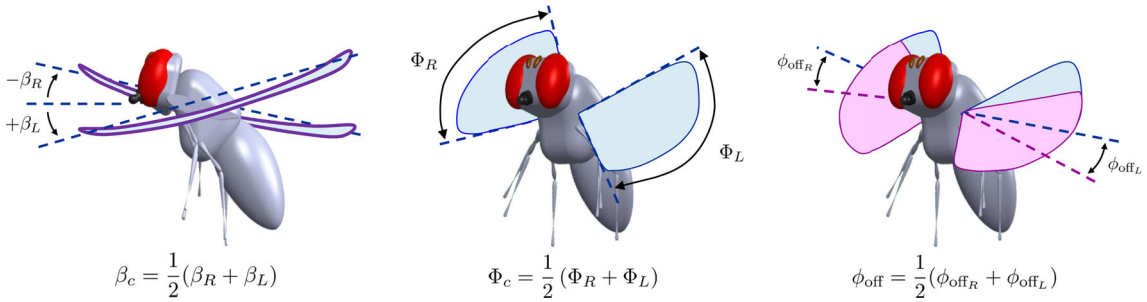

Fig. 5 Insect longitudinal flight control inputs are defined as gross wingstroke parameters

Table 1 State and control input definitions for the micro-quadrotor (MQ) and *Drosophila hydei* (DH) dynamics models

Vehicle	Signal	Value
MQ	$\mathbf{x}$	$[u, q, \theta]$
MQ	$\bar{\mathbf{x}}$	$[x_i, x, u, q, \theta]$
DH	$\mathbf{x}$	$[u, w, q, \theta]$
MQ	$\mathbf{u}$	$[\delta_{\text{lon}}]$
DH	$\mathbf{u}$	$[\Phi, \beta_c, \phi_{\text{off}}]$

3.4 Feedback control law extraction

By comparing the closed loop system in Sect. 3.3 against the open loop model developed in Sect. 3.1, the combined effects of feedback control may be determined. This section describes how this determination may be accomplished in a norm-minimizing sense. The extraction problem may be stated as follows: =

Given An open loop system $\dot{\mathbf{x}} = Ax + Bu$, $A \in \mathbb{R}^{n\times n}$, $B \in \mathbb{R}^{n\times p}$, and a corresponding closed loop dynamics matrix identified closed loop system $A_{\text{cl}} \in \mathbb{R}^{n\times n}$,

Find the linear state feeback law $\mathbf{u} = -K\mathbf{x}$ implemented by the closed loop system's controller.

Solution The closed loop dynamics matrix identified in Sect. 3.3 may be written as a function of the open loop system in Sect. 3.1 as

$$A_{\text{cl}} = A - BK \tag{4}$$

and solved for BK to yield a linear matrix equation

$$BK = A - A_{\text{cl}}. \tag{5}$$

In the typical case that where $n > p$, the linear matrix equation in K is overdetermined, and for $n > p$ and B full column rank, a solution for K satisfying (5) does not exist. However, a norm-minimizing gain matrix $\hat{K}$ may be computed via the generalized left inverse

$$B^{\dagger} = \left(B^{\mathrm{T}}B\right)^{-1} B^{\mathrm{T}} \tag{6}$$

by computing

$$\hat{K} = B^{\dagger}\left(A - A_{\text{cl}}\right). \tag{7}$$

$\hat{K}$ minimizes the normed residual such that

$$\left\| B\hat{K} - (A - A_{\text{cl}}) \right\|_{\text{F}} \leq \|BK - (A - A_{\text{cl}})\|_{\text{F}}, \tag{8}$$

where $\|\cdot\|_{\text{F}}$ denotes the Frobenius norm, defined by $\|M\|_{\text{F}} = \sqrt{\text{tr}(M^{*}M)}$.

While an extracted feedback control law $\hat{K}$ may be useful for implementation on a vehicle with the same configuration, it is not immediately clear what aspects of the overall closed loop performance the control law maximizes or how to implement the same control design strategy on a vehicle with different dynamics. Section 3.5 addresses this question by extracting optimality-based metrics.

3.5 Optimal control inversion

The inverse optimal control problem asks: Given an open loop system dynamics model and a feedback control law, what performance metric J (or cost functional $\ell(\mathbf{x}, \mathbf{u})$) does that feedback control law optimize? A more practical statement of the inverse control problem, as a function of measurements, is

> Determine the objective function $\ell(\mathbf{x}, \mathbf{u})$ that minimizes $J = \int \ell[\mathbf{x}(t), \mathbf{u}(t), t]\mathrm{d}t$ for a given set of state measurements $\mathbf{x}(t) \in \mathcal{L}_2$ and input measurements $\mathbf{u}(t) \in \mathcal{L}_2$, both recorded along some trajectory.

In this application, we will use the linear quadratic regulator form, which is a particular choice of $\ell(\mathbf{x}, \mathbf{u}) = \mathbf{x}^{\mathrm{T}}Q\mathbf{x} + \mathbf{u}^{\mathrm{T}}R\mathbf{u}$, for which the forward control problem statement is

LQR control problem Given an open loop system (A, B) and $Q \geq 0$, $R > 0$, $(\mathbf{x}, \mathbf{u}) \in \mathcal{L}_2$, with $(A, Q^{1/2})$ detectable, find the feedback gain $\mathbf{u} = -Kx$ that minimizes the cost

$$J = \int_0^{\infty} \mathbf{x}^{\mathrm{T}}(t)Q\mathbf{x}(t) + \mathbf{u}^{\mathrm{T}}(t)R\mathbf{u}(t).$$

The LQR control problem is an optimal control problem that has well-known analytic solutions. The associated inverse optimal control problem for the linear quadratic regulator is:

Inverse LQR problem Given an open loop system (A, B) and feedback gain $\hat{K}$, does there exist $\hat{Q} \geq 0, \hat{R} > 0, (\mathbf{x}, \mathbf{u}) \in \mathcal{L}_2$, with $(A, \hat{Q}^{1/2})$ detectable and for which $\mathbf{u} = -Kx$ minimizes the cost

$$J = \int_0^{\infty} \mathbf{x}^{\mathrm{T}}(t)\hat{Q}\mathbf{x}(t) + \mathbf{u}^{\mathrm{T}}(t)\hat{R}\mathbf{u}(t).$$

If so, compute $\hat{Q}$, $\hat{R}$.

Using the solution of the LQR optimal control problem, one may write constraints that the $\hat{Q}$ and $\hat{R}$ matrices must satisfy in order to be a solution of the inverse LQR problem.

$$(A - B\hat{K})^{\mathrm{T}}P + P(A - B\hat{K}) + \hat{K}^{\mathrm{T}}\hat{R}\hat{K} + \hat{Q} = 0, \tag{9}$$

$$P \geq 0, \hat{Q} \geq 0$$

$$B^{\mathrm{T}}P - \hat{R}\hat{K} = 0, \tag{10}$$

$$\hat{R} > 0$$

$$A^{\mathrm{T}} P_1 + P_1 A < \hat{Q}, \qquad P_1 > 0. \quad (11)$$

In the general case, $\hat{Q}$, $\hat{R}$ satisfying (9) through (11) may not exist, or may not be unique. Conditions for existence may be derived requiring (A, B) controllable and conditions on the cost $\ell(\mathbf{x}, \mathbf{u})$ and reachable states (Fujii and Narazaki 1984). In the case that $\hat{Q}$, $\hat{R}$ exist, they are likely not unique; i.e., there may be multiple $\hat{Q}$, $\hat{R}$ that yield the same gain matrix $\hat{K}$. Because diagonal terms have the most intuitive interpretation, we choose a linear objective function that yields the "maximally-diagonal" solution (Aïoun et al. 1994)

$$\min_{\hat{Q},\hat{R}} \bar{\sigma}\left(\hat{Q} - \mathtt{diag}(\hat{Q})\right) + \bar{\sigma}\left(\hat{R} - \mathtt{diag}(\hat{R})\right), \quad (12)$$

where $\bar{\sigma}(M)$ denotes the maximum singular value of a matrix M.

While the problem of minimizing the cost in Eq. (12) subject to Eq. (9) through (11) is solved numerically, it is a non-differentiable convex optimization problem and can be written as a system of linear matrix inequalities (LMIs). In the last 10–15 years, efficient solvers for these problems have become available, and the problem can be solved computationally efficiently with guarantees on both convergence and global optimality (Boyd et al. 1997). Because the LMIs in Eq. (9)–(11) and cost minimization in Eq. (12) correspond to an optimization over a self-dual homogenous cone, the self-dual embedding technique (Ye et al. 1994) as implemented in SeDuMi (Sturm 1999) allows efficient solutions or infeasibility certificates. The PenLab semidefinite optimization routine was applied because its implementation in open-source MATLAB® code provides a user-friendly flexibility to modify the underlying algorithms and build on this work (Fiala et al. 2013).

4 Simulation and experimental measurement

The optimal identification technique requires recorded time histories of the input and state trajectories. This section describes the acquisition of trajectories for the two examples, via simulation of microquad trajectories and via experimental measurement of insect flight trajectories.

4.1 Microquad trajectory simulation

4.1.1 Micro-quadrotor dynamics

The longitudinal open loop dynamics of the micro-quadrotor linearized about hover were identified, by using position tracking about hover. Step inputs, doublets, and frequency sweep rate inputs were applied to the vehicle in flight and both rigid body states and control input time histories were collected at 100 Hz using a Vicon motion capture arena. These responses were used to identify the dynamics of the system using least-squares and maximum likelihood estimator techniques. The resulting system is shown in Eq. (13) in state-space form, where $\delta_{\mathrm{lon}} \in [-1, 1]$ and is linearly related to a desired pitch rate.

$$\begin{bmatrix} \dot{u} \\ \dot{q} \\ \dot{\theta} \end{bmatrix} = \begin{bmatrix} -1.35 & 0.61 & -9.81 \\ 6.16 & -9.61 & -54.78 \\ 0 & 1 & 0 \end{bmatrix} \begin{bmatrix} u \\ q \\ \theta \end{bmatrix} + \begin{bmatrix} 0 \\ 50.44 \\ 0 \end{bmatrix} \delta_{\mathrm{lon}} \quad (13)$$

4.1.2 Optimal position tracking through LQR control

In order to design a position-referenced controller within the LQR framework, the open loop longitudinal hover dynamics are first augmented with the inertial position x and its integral x_i so that $\bar{\mathbf{x}} = [x_i, x, u, q, \theta]^{\mathrm{T}}$.

$$\begin{bmatrix} \dot{x_i} \\ \dot{x} \\ \dot{u} \\ \dot{q} \\ \dot{\theta} \end{bmatrix} = \begin{bmatrix} 0 & 1 & 0 & 0 & 0 \\ 0 & 0 & 1 & 0 & 0 \\ 0 & 0 & -1.35 & 0.61 & -9.81 \\ 0 & 0 & 6.16 & -9.61 & -54.78 \\ 0 & 0 & 0 & 1 & 0 \end{bmatrix} \begin{bmatrix} x_i \\ x \\ u \\ q \\ \theta \end{bmatrix} + \begin{bmatrix} 0 \\ 0 \\ 0 \\ 50.44 \\ 0 \end{bmatrix} \delta_{\mathrm{lon}} \quad (14)$$

The optimal position controller is designed as a regulator and then augmented with a new control sensitivity matrix E to rewrite the state dynamics in terms of error tracking a reference position. The final closed loop system, with input $\delta_{\mathrm{lon}} = -K\bar{\mathbf{x}}$, may then be written as

$$\dot{\bar{\mathbf{x}}} = (A - BK)\bar{\mathbf{x}} + Er, \quad (15)$$

where K is the LQR gain matrix, E the new closed loop control sensitivity matrix, and r the reference position, with full-state feedback used for this controller. By choice of E in Eq. (16), the controller acts on the error between the inertial position and reference position, and x_i state represents the integral of inertial position error.

$$E = \begin{bmatrix} -1 & 0 & 0 & 0 & 0 \end{bmatrix}^{\mathrm{T}} \quad (16)$$

$$e(t) = x(t) - r(t) \tag{17}$$

$$e_i(t) = \int_0^t e dt \tag{18}$$

4.1.3 LQR synthesis

Design Q_{in} and R_{in} weighting matrices for the flight controller were chosen as

$$Q_{\text{in}} = \begin{bmatrix} 10 & 0 & 0 & 0 & 0 \\ 0 & 10 & 0 & 0 & 0 \\ 0 & 0 & 5 & 0 & 0 \\ 0 & 0 & 0 & 1 & 0 \\ 0 & 0 & 0 & 0 & 1 \end{bmatrix}, \; R_{\text{in}} = 20, \tag{19}$$

and the solution of the associated algebraic Riccati equation resulted in the feedback gain

$$K = \begin{bmatrix} -0.7071 & -1.4536 & -0.6250 & 0.1853 & 1.7632 \end{bmatrix}. \tag{20}$$

The resulting closed loop system representing the microquadrotor, including position tracking LQR, is

$$\begin{bmatrix} \dot{x}_i \\ \dot{x} \\ \dot{u} \\ \dot{q} \\ \dot{\theta} \end{bmatrix} = \begin{bmatrix} 0 & 1 & 0 & 0 & 0 \\ 0 & 0 & 1 & 0 & 0 \\ 0 & 0 & -1.35 & 0.61 & -9.81 \\ 35.67 & 73.33 & 37.68 & -18.95 & -143.7 \\ 0 & 0 & 0 & 1 & 0 \end{bmatrix} \begin{bmatrix} x_i \\ x \\ u \\ q \\ \theta \end{bmatrix} + \begin{bmatrix} -1 \\ 0 \\ 0 \\ 0 \\ 0 \end{bmatrix} r \tag{21}$$

4.1.4 Closed loop simulation

The closed loop longitudinal system with LQR position controller implemented in (21) was simulated using MATLAB's `»lsim` command with a multi-step square wave position command (reference), as shown in Fig. 7. The resulting closed loop time histories were the data used as measurements for the micro quadrotor OID analysis, for which the longitudinal states (x_i, x, u, q, θ) were considered the outputs and the reference position command considered to be the closed loop input.

4.2 Drosophila experimental measurement

Ninety-two trajectories of free-flying *Drosophila* were collected using an automated high speed camera setup and image tracking software (Muijres et al. 2014). Biomechanical data

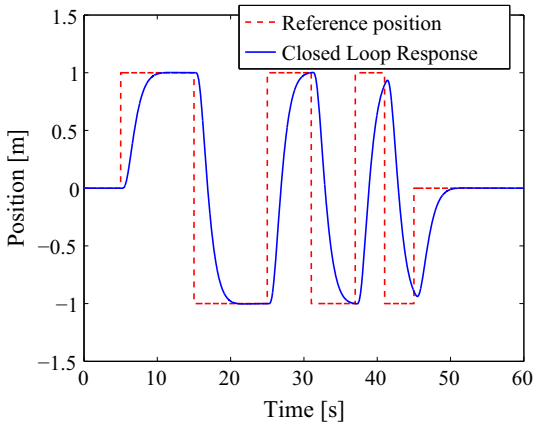

Fig. 7 Simulation of microquadrotor closed loop response to a multi-step position tracking command

were digitized at the video frame rate of 7500 Hz. While the majority of flight trials were aerobatic escape sequences, this study uses only sequences involving periods of straight and level forward flight, featuring small accelerations and low climb or descent speed. To accept a segment for analysis, deviations in pitch angle were required to be less than 12° and deviations from mean forward flight speed to not exceed 10% of the mean flight speed u_0 in the trial. The trial was terminated when an escape maneuver involving a yaw rate greater than 650°/s was detected.

System identification requires a continuous method of estimating the maneuvering control inputs to transform instantaneous wing quaternion measurements into gross wingstroke parameters, such as β, ϕ_{off}, and Φ that are discretized at measurement frequency. A least squares planar fit to a moving time window with the length of a single wingstroke was used to continuously estimate the wing stroke plane and the arctangent function used to extract a continuous time history of each wing's stroke plane angle β. Each wing's digitized (ϕ, θ) stroke variables were rotated by an angle $-\beta$ as

$$\begin{bmatrix} \gamma_{\text{L}} \\ \xi_{\text{L}} \end{bmatrix} = \begin{bmatrix} \cos\beta_{\text{L}} & -\sin\beta_{\text{L}} \\ \sin\beta_{\text{L}} & \cos\beta_{\text{L}} \end{bmatrix} \begin{bmatrix} \phi_{\text{L}} \\ \theta_{\text{L}} \end{bmatrix} \tag{22}$$

to reveal in and out-of plane motion. Here, γ_{L} represents in-plane motion of the left wing, and ξ_{L} is the left wing's out-of-plane motion. The in-plane component γ of each wing's motion was used to identify amplitude Φ and bias ϕ_{off} by peak and zero-crossing detection discretely and linearly interpolated to the sample frequency. The collective (symmetric) β_c, Φ, and ϕ_{off} perturbations from the trial's mean value were used as longitudinal control inputs for system identification. An example time history of β during a slalom is shown in Fig. 8, which was used as input to the *Drosophila* OID problem.

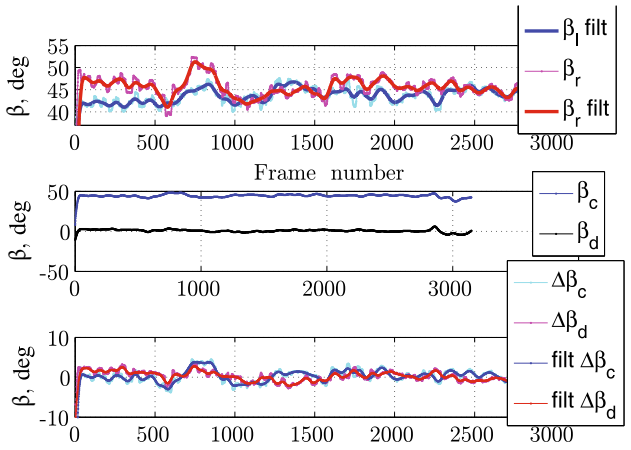

Fig. 8 Differential, and perturbations of stroke plane angle inputs for an example insect performing a slalom maneuver, digitized at 7500 Hz

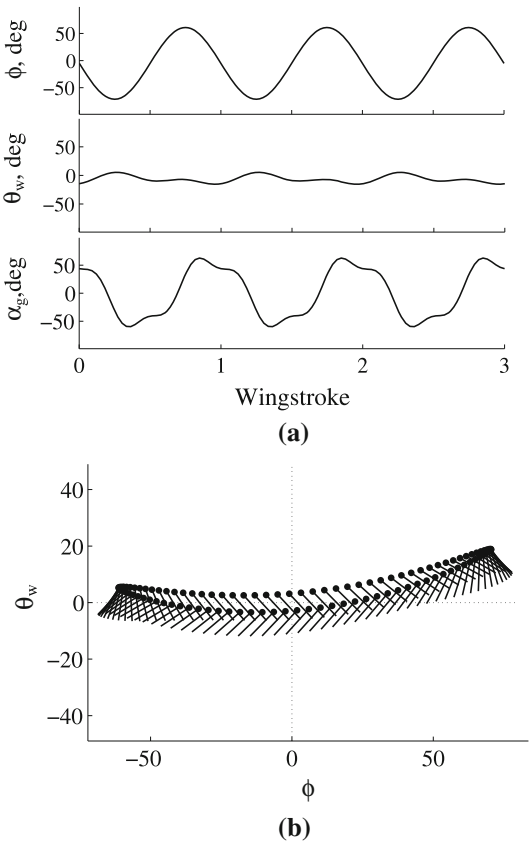

Fig. 9 Reference flight wing kinematics **a** over three wingstrokes and **b** in the phase plane

5 Results and discussion

5.1 Open loop flight dynamics modeling

5.1.1 Micro quadrotor open loop dynamics modeling

The micro-quadrotor dynamics shown in Eq. (13) were used as the open loop reference model to compare against for the microquadrotor control extraction task. Deviations from the behavior described by this open loop model were assumed to be due to closed loop control, which allowed the feedback control law $\hat{K}$ and its optimality conditions (Q_{in}, R_{in}) to be estimated.

5.1.2 Drosophila open loop QS modeling

An ensemble average of the measured insect wingstroke motions was used as reference wing motions to generate an open loop flight dynamics quasi-steady wingstroke model. Figure 9 shows the reference wing motions in the (3–1–2) rotation sequence $(\phi, \theta_w, \alpha_g)$ measurement terms most commonly used in insect flight measurement (Hedrick 2008; MacFarlane et al. 2015).

The estimated open loop *Drosophila* dynamics model is a linearized, wingstroke-averaged model based on a quasi-steady translational lift and drag force aerodynamics (Hedrick et al. 2009; Hedrick and Robinson 2010; Faruque and Humbert 2010a, b). The quasi-steady assumption models lift and drag as functions exclusively of the instantaneous air speed $\mathbf{U}_p(t)$ and angle of attack $\alpha_p(t)$ at a point on the wing.

Lift is modeled as a function of air density ρ, wing area S, and non-dimensional second moment of area $\hat{r}_2 = \int_0^1 \hat{c}\hat{r}^2 \mathrm{d}\hat{r}$ by

$$L(t) = \frac{1}{2}\rho \|\mathbf{U}_p(t)\|^2 S \hat{r}_2^2 C_{\text{L}}(\alpha_p(t)), \tag{23}$$

where $\hat{\text{c}}$ and $\hat{\text{r}}$ are normalized chord and radius, respectively. Drag is similarly modeled with a drag coefficient C_{D}. Both lift and drag coefficients are curve fits to experimental data (Fry et al. 2003) using RoboFly.

Local wing motion is assumed to be wing rotation and body translation and rotation expressed into the wing frame as a function of wing angular rate $\boldsymbol{\omega}_{\text{w}}$, body angular rate $\boldsymbol{\omega}_{\text{b}}$, body translational rate $\mathbf{v}_{\text{b}}$, and the vector from the CG to the point on the wing $\mathbf{R}_p$:

$$\begin{aligned}\left[\mathbf{U}_p(t)\right]_{\text{w}} = {} & \boldsymbol{\omega}_{\text{w}}(t) \times \left[\mathbf{R}_p\right]_{\text{w}} + \left[\mathbf{v}_{\text{b}}(t)\right]_{\text{w}} \\ & + \left[\boldsymbol{\omega}_{\text{b}}(t) \times \left[\mathbf{R}_p(t)\right]_{\text{b}}\right]_{\text{w}},\end{aligned} \tag{24}$$

where $[\cdot]_{\text{b}}$ indicates a vector expressed in wing frame coordinates and $[\cdot]_{\text{w}}$ indicates wing frame coordinates. Angle of attack α_p is

$$\alpha_p(t) = \tan^{-1}\left(\frac{\mathbf{U_p}(t) \cdot \hat{p}_3}{\mathbf{U_p}(t) \cdot \hat{p}_1}\right). \tag{25}$$

Given a set of wing and body kinematics, the quasi-steady aerodynamics model predicts flapping wing aerodynamic forces with only modest computational expense. The experimentally-determined lift and drag curves incorporate some aerodynamics effects, such as three dimensional effects of a rotating wing and leading edge and tip vortex interaction, but neglect added mass, rotational lift, and wake capture effects.

Using small disturbance theory, the resulting nonlinear system of ordinary differential equations describing the flight dynamics may be reduced to a linear, time periodic system. In vehicle flight dynamics analysis, results from averaging theory suggest that the long term, low frequency evolution of body motion may be described using the stroke-averaged aerodynamic forces (Vela and Burdick 2003). For the *Drosophila* insect considered here, the wing flapping frequency (200 Hz) is more than 10 times the frequency of the fastest rigid body natural mode (about 6 Hz Graetzel et al. 2010). For larger insects, the frequency separation assumption must be examined (Wu and Mao 2012).

Wingstroke-averaged aerodynamic forces are then used for the calculation of the stability and control derivatives A, B. The stroke-averaged forces are $\bar{\mathbf{F}} = \frac{1}{T}\int_0^{\mathrm{T}} \mathbf{F}(t)\mathrm{d}t$, where $\mathbf{F}(t) = [X(t),\ Y(t),\ Z(t)]^{\mathrm{T}}$ is periodic at wingstroke period T. The result is a linear, time invariant (LTI) model that estimates the flight dynamics of the insect, and is applicable for control analysis. The derived *Drosophila* open loop LTI flight dynamics model is $\dot{\mathbf{x}} = A\mathbf{x} + B\mathbf{u}$, where $\mathbf{x} = \begin{bmatrix} u & w & q & \theta \end{bmatrix}^{\mathrm{T}}$, $\mathbf{u} = \begin{bmatrix} \Phi & \beta_c & \phi_{\mathtt{off}} \end{bmatrix}^{\mathrm{T}}$, and

$$A = \begin{bmatrix} -4.017 & -0.0212 & 0.002 & -9.81 \\ 0.1188 & -4.14 & 0.0227 & 0 \\ 6281.0 & 7161.0 & -29.8 & 0 \\ 0 & 0 & 1.0 & 0 \end{bmatrix},$$

$$B = \begin{bmatrix} 0.3555 & 10.01 & 0.3766 \\ -16.83 & -0.0855 & -0.0138 \\ 31066.0 & -14399.0 & 59088.0 \\ 0 & 0 & 0 \end{bmatrix}. \tag{26}$$

5.2 Closed loop system identification

5.2.1 Microquadrotor

The closed loop simulation data were used to identify an estimate of the closed loop system using least squares linear regression. The states of the simulated closed loop system are shown in Fig. 10 and were used as the regressors for the least squares identification. The computed state derivatives are shown in Fig. 11 and formed the measured output vector for the linear regression.

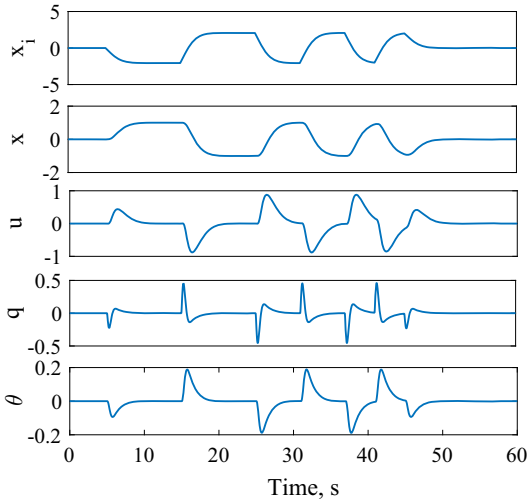

Fig. 10 Time history of microquadrotor states from closed loop simulation

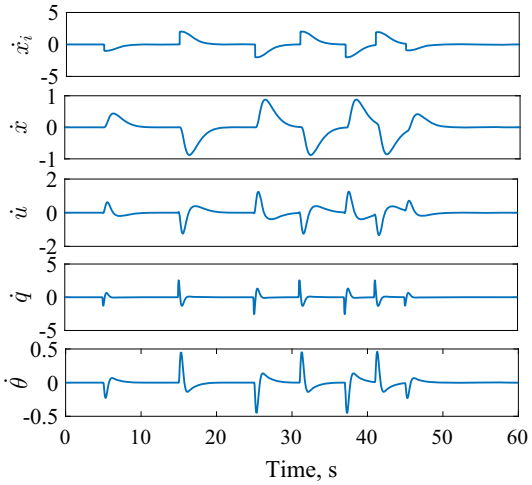

Fig. 11 Time history of micro quadrotor state derivatives from closed loop simulation

The identified closed loop model

$$\begin{bmatrix} \dot{x}_i \\ \dot{x} \\ \dot{u} \\ \dot{q} \\ \dot{\theta} \end{bmatrix} = \begin{bmatrix} 0 & 1 & 0 & 0 & 0 \\ 0 & 0 & 1 & 0 & 0 \\ 0 & 0 & -1.35 & 0.61 & -9.81 \\ 35.48 & 72.93 & 37.47 & -18.84 & -142.98 \\ 0 & 0 & 0 & 1 & 0 \end{bmatrix} \begin{bmatrix} x_i \\ x \\ u \\ q \\ \theta \end{bmatrix} + \begin{bmatrix} -1 \\ 0 \\ 0 \\ 0 \\ 0 \end{bmatrix} r$$

compares well to the idealized closed loop dynamics. To validate the identified model, the computed and identified models were simulated in response to a different input type

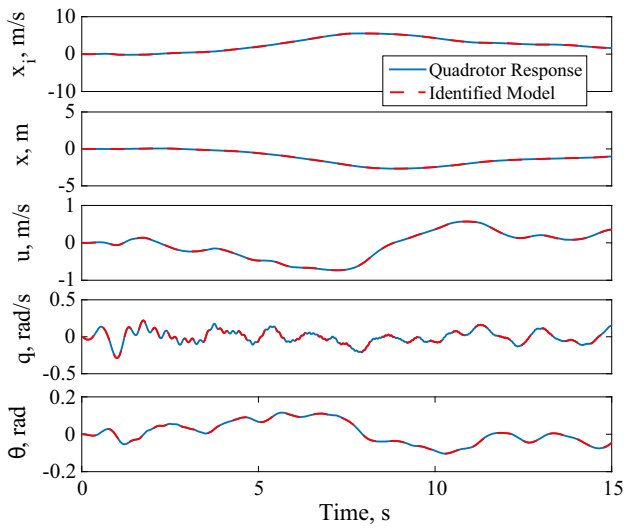

Fig. 12 Identified closed loop microquadrotor model validation using a noisy chirp signal

(noise and chirp signal) and the comparison seen in Fig. 12 shows excellent agreement.

5.2.2 Drosophila

Time domain system identification was also conducted on each insect flight segment meeting the acceptance requirements in Sect. 3. 4.2. Matched filtering, consisting of a moving average with window size corresponding to the detected wingbeat frequency, was first applied to inputs and outputs to reduce high frequency measurement noise. Time domain system identification was conducted using equation error methods in SIDPAC (Klein and Morelli 2002). An example fit for the trial at $u_0 = 368$ mm/s can be seen in Fig. 13, which shows good agreement between measured data and simulated time histories generated by running the identified model. The linear-time invariant model is not able to capture the low-amplitude, high frequency wingstroke oscillations in pitch rate that would require time varying or periodic models, but are not likely to form the bulk of the feedback path in larger scale flight control.

The identified model has a closed loop dynamics matrix

$$A_{\mathrm{cl}} = \begin{bmatrix} -511.4 & 174.7 & 0 & -9.806 \\ 1795.0 & -697.7 & 368.4 & 0 \\ 1.542 & 0.6319 & -37.9 & 0 \\ 0 & 0 & 1.0 & 0 \end{bmatrix}, \tag{27}$$

which indicates that closed loop control acts to increase damping on all the longitudinal axes.

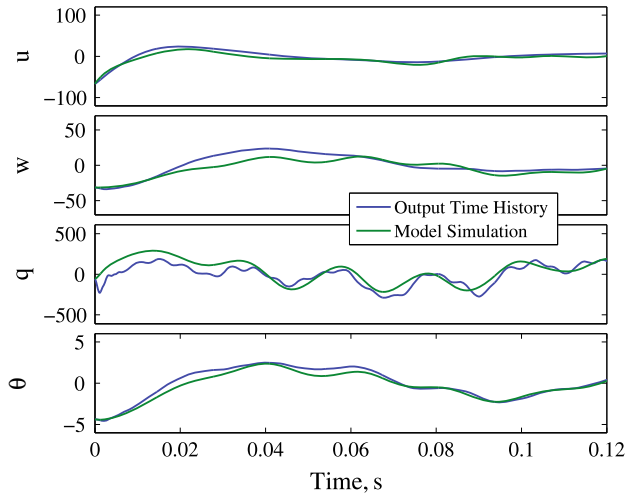

Fig. 13 The closed loop *Drosophila* system identification fit compares well to the recorded flight trials

5.3 Feedback control law extraction

5.3.1 Micro quadrotor

The insect's longitudinal feedback control law is extracted using the Frobenius norm minimizing method discussed in Sect. 3. 3.4. In particular, Eq. (7) estimates the feedback gain

$$\hat{K}_{\mathrm{mq}} = \delta_{\mathrm{lon}} \overset{x_i}{\underset{}{\left[-0.7033 \right.}} \overset{x}{\underset{}{-1.446}} \overset{u}{\underset{}{-0.6208}} \overset{q}{\underset{}{0.1831}} \overset{\theta}{\underset{}{\left. 1.748 \right]}}. \tag{28}$$

When the gain estimate is compared to the true gain in Eq. (20), the estimated gains show very good agreement, with deviations ranging from 0.54 to 1.16%.

5.3.2 Insect

The insect's longitudinal feedback control law is extracted using the same Frobenius norm minimizing method used on the microquadrotor, but applied to each individual trial. For example,

$$\hat{K} = \begin{matrix} \\ \phi_c \\ \beta_c \\ \phi_{\mathrm{off,c}} \end{matrix} \overset{\begin{matrix} u & w & q & \theta \end{matrix}}{\begin{bmatrix} 106.5 & -41.15 & 21.91 & 1.831 \times 10^{-6} \\ 48.57 & -16.67 & -0.3413 & -0.0003465 \\ -44.06 & 17.7 & -11.6 & -8.536 \times 10^{-5} \end{bmatrix}} \tag{29}$$

is the identified feedback control law for the trial with mean forward flight speed $u_0 = 368.4$ mm/s. While this feedback gain estimate is useful for estimating the sensing requirements for feedback on insects, and could be implemented on a bio-mimetic flapping wing micro-aerial vehicle having wing

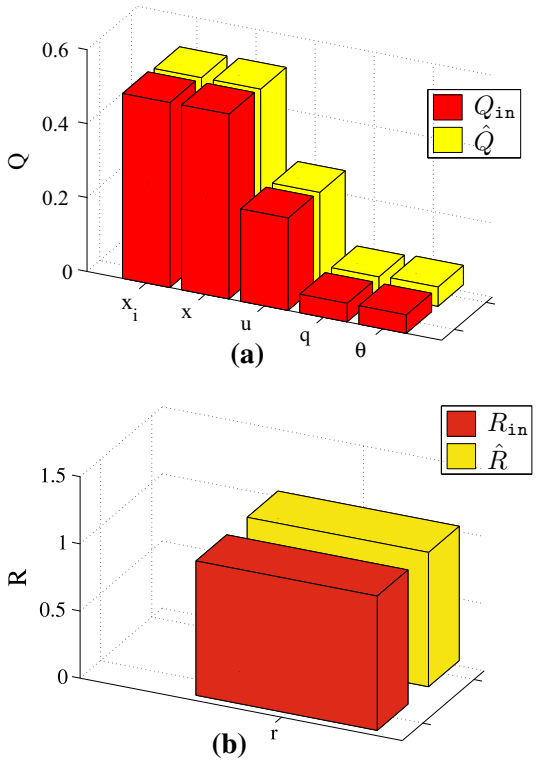

Fig. 14 OID estimates the quadrotor $\hat{Q}$, $\hat{R}$ matrices very well when compared to the input design matrices, with a mean identification error of 2.1%

kinematic motion programs that implement the same stroke amplitude, bias and stroke plane angles as control inputs, a more general interpretation may be found by considering the role of dynamics and extracting optimal feedback design rules, a task addressed in Sect. 5.4.

5.4 Optimality principles

5.4.1 Micro quadrotor optimality principles

The optimal quadrotor matrices were extracted as

$$\hat{Q} = \begin{bmatrix} 0.49 & 0 & 0 & 0 & 0 \\ 0 & 0.49 & 0 & 0 & 0 \\ 0 & 0 & 0.25 & 0 & 0 \\ 0 & 0 & 0 & 0.049 & 0 \\ 0 & 0 & 0 & 0 & 0.052 \end{bmatrix}, \tag{30}$$

where $\hat{Q}$ has been normalized by $\hat{R}$ to resolve the ambiguity in scale and any terms smaller than 1×10^{-17} were considered zero. Figure 14 shows that the identified $\hat{Q}/\hat{R}$ ratio compares well to the design Q/R ratio from Eq. 19, with nonzero terms showing identification errors ranging from 1.1 to 4.4% of the correct value, and a mean identification error of 2.1%.

5.4.2 Drosophila optimality principles

The optimality metrics for the insect flight control law are extracted via the maximally-diagonal inverse LQR method as

$$\hat{Q} = \begin{bmatrix} u & w & q & \theta \\ 8.95 & -1.91 & -0.91 & 0.0030 \\ -1.91 & 0.54 & -2.90 & -0.0033 \\ -0.91 & -2.90 & 29.15 & -1.60 \\ 0.0030 & -0.0033 & -1.604 & 0.25 \end{bmatrix},$$

$$\hat{R} = \begin{bmatrix} \Phi & \beta_c & \phi_{off} \\ 0.43 & -0.054 & 1.08 \\ -0.054 & -0.23 & -0.41 \\ 1.08 & -0.41 & 2.34 \end{bmatrix} \tag{31}$$

for the example forward flight speed u_0 =368.4 mm/s. The relative weights of the quadratic costs involving each state are shown in Fig. 15a for several sequences at varying forward flight speeds from 152 to 571 mm/s. The results indicate that, in most trials, the combined effect of the insect flight control

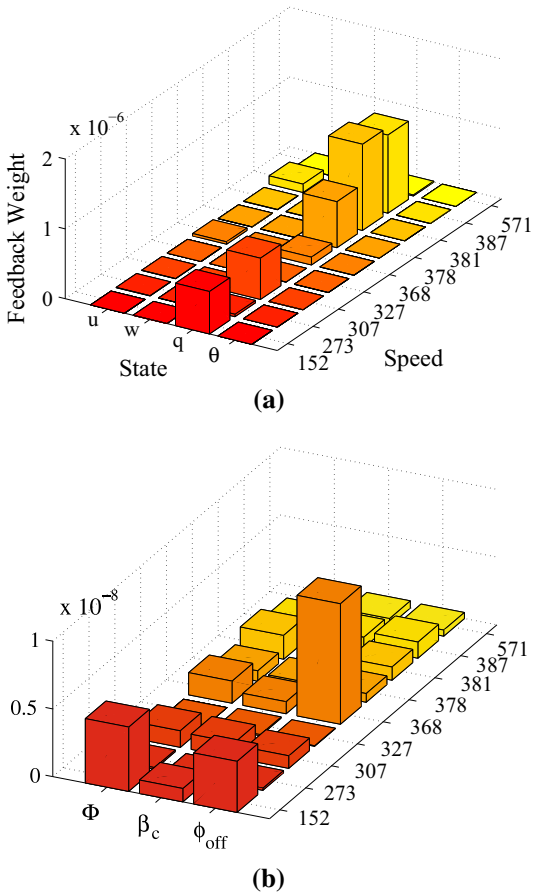

Fig. 15 Feedback control law optimality metrics for longitudinal state ($\hat{Q}$) and control ($\hat{R}$) in *Drosophila* for varying flight speeds u_0 indicate that deviations in pitch rate are penalized more strongly than other states

law penalizes pitch rate deviations most strongly. The finding that the composite feedback system penalizes pitch rate deviations most strongly is supported by engineered and biological studies that have found numerous sensor structures capable of encoding pitch rate, including mechonosensory (haltere) feedback, optic flow (lobula plate tangential cell), and fixed focus simple eyes (ocellar) mechanisms. In contrast, the suite of sensors available to the insect to encode and feed back other states, such as orientation, distance, or translational rates, is more limited. The relative weights of the quadratic cost involving each input are shown in Fig. 15b, indicating that the recorded trials selected show diversity of willingness to expend control effort.

As opposed to the feedback control law in Sect. 5.3, the optimality conditions presented here could allow us to implement the identified feedback control principle on a platform with different dynamics, e.g., translating insect-based feedback control laws to a micro-quadrotor platform through LQR control. Although the feedback implemented on the insect may not, in general, represent an engineered system explicitly designed using LQR control, the use of inverse LQR is appropriate for controllers that can be written as a linear static gain, since the implementations of many linear control techniques (e.g., pole placement, PID) have equivalents in LQR design space which are found using the optimal identification method. These LQR-equivalents are useful for interpreting a particular control law or for generating a parallel implementation that penalizes similar inputs.

5.5 Discussion of limitations, assumptions, and future improvements

While the study began with analysis of 1,542,288 video frames, of which an insect was robustly tracked in 459,303 frames containing 92 digitized flight sequences, each including an escape maneuver response to stimulus, the diversity of behaviors within the flight trials was not designed for identifying sequences that consist of small deviations about a straight and level flight, thus only 11 trials contained sections of straight flight, which were at varying flight speeds and were limited to portions of the trial prior to the large deviations found in escape sequences. Because the insect was not reacting to a known stimulus in this period, the trials studied represent a cross section of both individual insects and potentially varying behaviors, limiting the ability to validate insect system identifications. Given the lack of a strong stimulus to induce a behavior and the range of speeds covered in the analyzed trials, the consistency in strong pitch rate feedback is remarkable, but the range of behaviors may have led to a spread in the control effort results. Based on the success with accurately and repeatedly identifying the microquadrotor dynamics where researchers have more control over the flight test structure, an experimental study explicitly designed to digitize insects making small maneuvers about straight and level flight may be useful in focusing the analysis on a specific behavior and increasing the precision of results.

The *Drosophila* insect dynamics matrices also have a large condition number, and large scale ratios can cause numerical sensitivities with the pseudo inverse and linear matrix inequality portions of the method. The numerical properties of the solution may be addressed by state-scaling or normalization of states in order to improve the condition number of the matrices. However, scaling does have the effect of obscuring the units on $\hat{Q}$, $\hat{R}$, especially the off-diagonal terms, and a thorough treatment of scaling effects is reserved for a future study.

Insect feedback control laws need not necessarily be optimal with respect to the states chosen in this formulation, and they are not constrained to linear behavior. For the cases in which insect strategies may be regarded as optimal, the optimality may be with respect to states that are not accessible to current free flight measurement technologies, such as physiological variables or internal neuronal states. The linear analysis conducted herein assumes a structure on the optimal performance index J, and there may be value in considering more complex cost functions for which the inverse optimal problem may not be convex. However, the current analysis is not limited to feedback controllers developed through optimal control mechanisms. Instead, it provides a mechanism to interpret the effects of linear static gain feedback strategies $\hat{K}$. Insects may adapt their feedback optimality conditions over time and may also show variations over (among other parameters) species, individual, or life stage. OID presents a concise method to evaluate these changes over time and individual and to build physically intuitive, mathematically rigorous models of insect feedback control.

6 Conclusions

This paper presented an "optimal identification" (OID) technique for identifying the optimality conditions associated with a given control law by comparing closed loop trajectory information against an open loop dynamics model. The technique involves four components, including open loop plant modeling, closed loop system identification, feedback gain extraction, and inverse optimal control. The OID technique was then applied to the two examples of a micro-quadrotor with a known LQR controller, and a freely flying *Drosophila hydei* maneuvering about forward flight. The results provided an extracted flight control law, which in the quadrotor case, had a mean deviation of 2.1% from the input design variables. When OID was applied to free flying insect trajectories, it indicated that the combined effect of the insect longitudinal sensing and feedback control law is primarily to regulate pitch rate, a finding which can help to explain the effects of

insect sensory systems that have numerous sensors that each encode angular rotation rates. The identification of the overall performance targets with which the insect flight feedback system is optimal can help give MAV designers a composite closed loop performance strategy to robustly stabilize small vehicles in uncertain environments. Because of the maturity of optimal controller designs such as LQR, the OID approach can be used to understand the sensing requirements of an insect's feedback strategy, and to eventually generate engineered controllers that are tuned to achieve the same closed loop performance targets.

References

Aïoun F, Heniche A, Bourlès H (1994) Maximally-diagonal solution to the inverse LQR problem. In: Proceedings of the 33rd conference on decision and control, pp 1445–1446

Beatus T, Guckenheimer JM, Cohen I (2015) Controlling roll perturbations in fruit flies. J R Soc Interface 12(105):20150075

Boyd S, Ghaoui LE, Feron E, Balakrishnan V (1997) Linear matrix inequalities in system and control theory (studies in applied and numerical mathematics). Society for Industrial and Applied Mathematics, Philadelphia

Camhi JM (1970) Yaw-correcting postural changes in locusts. J Exp Biol 52(3):519–531

Cheng B, Fry SN, Huang Q, Deng X (2010) Aerodynamic damping during rapid flight maneuvers in the fruit fly drosophila. J Exp Biol 213:602–612

Conroy J, Gremillion G, Ranganathan B, Humbert JS (2009) Implementation of wide-field integration of optic flow for autonomous quadrotor navigation. J Exp Biol 27:189–198

David CT (1978) The relationship between body angle and flight speed in free-flying drosophila. Physiol Entomol 3(3):191–195

Dickinson MH (1990) Comparison of encoding properties of campaniform sensilla on the fly wing. J Exp Biol 151(1):245–261

Dickinson MH, Lighton JR (1995) Muscle efficiency and elastic storage in the flight motor of drosophila. Science 268(5207):87

Dickinson MH, Muijres FT (2016) The aerodynamics and control of free flight maneuvers in drosophila. Philos Trans R Soc B 371(20150388)

Dickinson MH, Tu MS (1997) The function of dipteran flight muscle. Comp Biochem Physiol A Physiol 116(3):223–238

Dickinson MH, Lehmann FO, Sane SP (1954) Wing rotation and the aerodynamic basis of insect flight. Science 284:1999

Eberle A, Dickerson B, Reinhall PG, Daniel T (2015) A new twist on gyroscopic sensing: body rotations lead to torsion in flapping, flexing insect wings. J R Soc Interface 12(104):20141088

Faruque IA, Humbert JS (2010a) Dipteran insect flight dynamics .Part 2: lateral–directional motion about hover. J Theor Biol 265(3):306–313

Faruque IA, Humbert JS (2010b) Dipteran insect flight dynamics. Part 1: longitudinal motion about hover. J Theor Biol 264(2):538–552

Fiala J, Kocvara M, Stingl M (2013) PENLAB: a MATLAB solver for nonlinear semidefinite optimization. arXiv preprint arXiv:1311.5240

Fry SN, Sayaman R, Dickinson MH (2003) The aerodynamics of free-flight maneuvers in Drosophila. Science 300(5618):495–498

Fujii T, Narazaki M (1984) A complete optimality condition in the inverse problem of optimal control. SIAM J Control Optim 22(2):327–341

Gao N, Aono H, Liu H (2011) Perturbation analysis of 6DoF flight dynamics and passive dynamic stability of hovering fruit fly Drosophila Melanogaster. J Theor Biol 270:98–111

Götz KG (1968) Flight control in drosophila by visual perception of motion. Kybernetik 4(6):199–208

Götz KG (1987) Course-control, metabolism and wing interference during ultralong tethered flight in drosophila melanogaster. J Exp Biol 128(1):35–46

Graetzel CF, Nelson BJ, Fry SN (2010) Frequency response of lift control in Drosophila. J R Soc Interface 7(52):1603–1616

Hedrick TL (2008) Software techniques for two- and three-dimensional kinematic measurements of biological and biomimetic systems. Bioinspir Biomim 3(3):034001

Hedrick TL, Robinson AK (2010) Within-wingbeat damping: dynamics of continuous free-flight yaw turns in Manduca sexta. Biol Lett 6:422–425

Hedrick TL, Cheng B, Deng X (2009) Wingbeat time and the scaling of passive rotational damping in flapping flight. Science 324:252–255

Heisenberg M, Wolf R (2013) Vision in Drosophila: genetics of microbehavior, vol 12. Springer, Berlin

Kalman RE (1964) When is a linear control system optimal. J Basic Eng 86D:51–60

Kennedy J (1983) Zigzagging and casting as a programmed response to wind-borne odour: a review. Physiol Entomol 8(2):109–120

Krapp HG (2009) Ocelli. Curr Biol 19(11):R435–R437

MacFarlane K, Bush B, Faruque I, Humbert JS, Baeder J (2011) Quasi-steady and computational aerodynamics applied to hovering *Drosophila* dynamics. In: AIAA 29th applied aerodynamics conference, June 2011. Honolulu, Hawaii, No. 2011-3793

MacFarlane KM, Faruque IA, Humbert JS (2015) Power regulation of kinematic control inputs for forward flying Drosophila. Acta Mech Sin 30(6):809–818

Klein V, Morelli E (2002) Aircraft system identification: theory and practice. In: AIAA

Muijres FT, Elzinga MJ, Melis JM, Dickinson MH (2014) Flies evade looming targets by executing rapid visually directed banked turns. Science 344:172

Muijres FT, Elzinga MJ, Iwasaki NA, Dickinson MH (2015) Body saccades of drosophila consist of stereotyped banked turns. J Exp Biol 218(6):864–875

Pringle JWS (1948) The gyroscopic mechanism of the halteres of diptera. Philos Trans R Soc Lond B Biol Sci 233(602):347–384

Ristroph L, Bergou AJ, Ristroph G, Coumes K, Berman GJ, Guckenheimer J, Wang ZJ, Cohen I (2010) Discovering the flight autostabilizer of fruit flies by inducing aerial stumbles. Proc Nat Acad Sci 107(11):4820–4824

Ristroph L, Ristroph G, Morozova S, Bergou AJ, Chang S, Guckenheimer J, Wang ZJ, Cohen I (2013) Active and passive stabilization of body pitch in insect flight. J R Soc Interface 10(85):20130237

Sane SP (2003) The aerodynamics of insect flight. J Exp Biol 206:4191–4208

Sane SP, Dieudonné A, Willis MA, Daniel T (2007) Antennal mechanosensors mediate flight control in moths. Science 315(5813):863–866

Schneider D (1964) Insect antennae. Annu Rev Entomol 9(1):103–122

Sherman A, Dickinson MH (2003) A comparison of visual and haltere-mediated equilibrium reflexes in the fruit fly Drosophila melanogaster. J Exp Biol 206:295–302

Sherman A, Dickinson MH (2004) Summation of visual and mechanosensory feedback in Drosophila flight control. J Exp Biol 207:133–142

Sturm JF (1999) Using SeDuMi 1.02, a MATLAB toolbox for optimization over symmetric cones. Optim Methods Softw 11(1–4):625–653

Straw AD, Lee S, Dickinson MH (2010) Visual control of altitude in flying drosophila. Curr Biol 20(17):1550–1556

Sun M, Wang J, Xiong Y (2007) Dynamic flight stability of hovering insects. Acta Mech Sin 23:231–246

Taylor GK, Thomas ALR (2003) Dynamic flight stability in the desert locust Schistocerca gregaria. J Exp Biol 206:2803–2829

Thompson RA, Wehling MF, Evers J (2008) Evaluation of the haltere as a biologically inspired inertial rate measurement sensor. In: Guidance, navigation, and control conference

van Breugel F, Dickinson MH (2012) The visual control of landing and obstacle avoidance in the fruit fly drosophila melanogaster. J Exp Biol 215(11):1783–1798

van Breugel F, Dickinson MH (2014) Plume-tracking behavior of flying drosophila emerges from a set of distinct sensory-motor reflexes. Curr Biol 24(3):274–286

Vela PA, Burdick JW (2003) Control of biomimetic locomotion via averaging theory. In: Proceedings of the IEEE international conference on robotics and automation, 2003, ICRA'03, vol 1, pp 1482–1489

Wehner R (1981) Spatial vision in arthropods. In: Autrum H (ed) Handbook of sensory physiology, vol 7/6C. Springer, Berlin, pp 287–616

Weis-Fogh T (1949) An aerodynamic sense organ stimulating and regulating flight in locusts. Nature 164(4177):873. https://doi.org/10.1038/164873a0

Wu JH, Mao S (2012) Floquet stability analysis of the longitudinal dynamics of two hovering model insects. J R Soc Interface 9(74):2033–2046

Ye Y, Todd MJ, Mizuno S (1994) An O (nL)-iteration homogeneous and self-dual linear programming algorithm. Math Oper Res 19(1):53–67